POST-PRINT

Submitted, accepted and published in

Fuel 111, 778-783 (2013); DOI: 10.1016/j.fuel.2013.05.001

CH_4 and CO_2 partial pressures influence and deactivation study on the Catalytic Decomposition of Biogas over a Ni catalyst.

S. de Llobet[a], J.L. Pinilla[a], M.J. Lazaro[a], R. Moliner[a], I. Suelves[a,*]

[a]*Instituto de Carboquímica (CSIC). C/ Miguel Luesma 4. 50018 Zaragoza, Spain*

e-mail: isuelves@icb.csic.es

Abstract

A conceptually similar approach to dry reforming of CH_4 (DRM) called Catalytic Decomposition of Biogas (CDB) is proposed. CDB is based on the direct decomposition of CH_4 and CO_2, which are the most abundant components in biogas (typically with CH_4:CO_2 molar ratios higher than 1). The main difference between DRM and CDB lies in the desired products obtained in each process. While in DRM carbon formation is not desired and thus avoided, in CDB carbon accumulation in form of filamentous structures is promoted. In this work, the effect of CH_4 and CO_2 partial pressures on the initial reaction rates of CDB was studied using a Ni/Al_2O_3 catalyst. Furthermore, a deactivation study was carried out in order to determine the experimental conditions (CH_4 and CO_2 partial pressures and temperature) at which carbon formation did not deactivate the catalyst. It was proved that after a certain time on stream, CDB can reach the steady state even though the CH_4:CO_2 molar ratio is higher than one (typical biogas conditions). In addition, temperature increased reaction rates since CDB is an endothermic process, but it had no effect on catalyst deactivation.

Keywords: Catalytic Decomposition of Biogas, CH_4-CO_2 reaction, Ni/Al_2O_3 catalyst, deactivation study, nanostructured carbon.

1 Introduction

Due to the finite nature of fossil fuels, it is necessary to change from our current energy system to a new long term sustainable system in which all the energetic sources should be considered. Biogas, a gas composed mainly of methane (40-70%) and carbon dioxide (30-60%) [1], can be used as feedstock in the dry reforming of CH_4 (DRM) to produce syngas and because of its renewable character, the process is classified as CO_2 neutral.

DRM ($CH_4 + CO_2 \rightarrow 2H_2 + 2CO$) is a highly endothermic reaction ($\Delta H^o = 247$ kJ·mol^{-1}) that takes place catalytically in a temperature range between 600-800 °C, producing a syngas with a theoretical H_2:CO molar ratio of 1:1 [2-10]. Nowadays, a general rate expression is not yet established for the CH_4-CO_2 reaction and different expressions can be found in the literature [11-16]. However, there is a general consensus on the elementary reaction steps [17]: CH_4 decomposition takes place on the leading face of the catalyst particle (active face), initially generating CH_x^* species and then chemisorbed carbon (C^*) and atomic hydrogen (H^*) {1-3}. At the same time, direct CO_2 decomposition {4} takes place followed by C^* and CH_x^* oxidation {5-6}, CO generation {7-8}, H_2 generation {9} and the reverse water gas shift reaction {10}.

$CH_4 \rightarrow CH_3^* + H^*$ {1}

$CH_x^* \rightarrow CH_{x-1}^* + H^*$ {2}

$CH^* \rightarrow C^* + H^*$ {3}

$CO_2 \leftrightarrow CO^* + O^*$ {4}

$C^* + O^* \leftrightarrow CO^*$ {5}

$CH^* + O^* \leftrightarrow CHO^*$ {6}

$CHO^* \leftrightarrow CO^* + H^*$ {7}

$CO^* \leftrightarrow CO$ {8}

$2H^* \leftrightarrow H_2$ {9}

$CO_2 + H_2 \leftrightarrow H_2O + CO$ {10}

Generally, when CH_4-CO_2 reaction is studied, efforts are devoted to avoid carbon formation in order to disregard its possible effects on the catalyst behaviour. Recently, a conceptually similar approach to DRM called Catalytic Decomposition of Biogas (CDB) has been proposed [18, 19]. CDB basically consists on the direct decomposition of CH_4 and CO_2 mixtures and comprises the main reaction steps considered for the DRM. The main difference between DRM and CDB lies in the desired products obtained in each process. As opposed to DRM reaction, CDB promotes carbon growth under optimized conditions in form of filamentous structures such as carbon nanofibers (CNF) that allow carrying out the reaction without catalyst deactivation. For that reason, another step on the mechanistic scheme of the CH_4-CO_2 reaction is added when using a Ni catalyst: C^* diffusion and precipitation on the trailing face of the catalyst particles to form filamentous carbon structures {11} [20]. It is generally accepted that C^* diffusion through the catalyst particle is the rate determining step in the growth of filamentous carbon [21].

$C^* \rightarrow C_{filamentous}$ {11}

Catalyst deactivation occurs when C^* produced after the breaking of the four C-H bonds of CH_4 {1-3} and located on the leading face of a catalyst particle is not able to diffuse to the trailing face {11} or to be oxidized with atomic oxygen (O^*) {5-6}. As a result, C^* accumulation takes place on the leading face, encapsulating catalyst particles.

However, if the different reaction rates involved in the process (equations {3}, {5} and {11}) are well balanced, then filamentous carbon structures may growth without catalyst deactivation.

In this work, two different approaches regarding the CH_4-CO_2 reaction are analysed. Firstly, reaction rates were calculated at the beginning of the reaction, when carbon accumulation on the leading face of the catalyst particles can be considered negligible and therefore the effect of CH_4 and CO_2 partial pressures on the reaction rates can be analyzed. Secondly, the evolution of reaction rates at longer reaction times was considered. As the reaction takes place, carbon formation starts to influence on the catalyst behaviour. Depending on the experimental conditions (CH_4 and CO_2 partial pressures and temperature) deactivation of the catalyst may occur. For that reason, it is necessary to understand under which experimental conditions is possible to promote the formation of filamentous carbon structures avoiding catalyst deactivation.

2 Experimental

2.1 Catalyst preparation

A Ni based catalyst using Al_2O_3 as textural promoter with a Ni:Al molar ratio of 2:1, previously developed for the Catalytic Decomposition of Methane ($CH_4 \rightarrow 2H_2 + C$) (CDM) by our research group [22] and denoted as Ni/Al_2O_3, was prepared by the fusion method previously described in [23]: briefly, nitric salts of nickel and aluminium were crushed, followed by the decomposition of the mixture at 350 °C for 1h and calcination at 450 °C for 8h. The powder sample was ground and sieved to allow the selection of different particle sizes: >40, 40-100 and 100-200 μm. The nickel domain size of the calcined fresh catalyst was 19 nm while after the reduction pre-treatment (under a H_2

flow at 550 °C) and passivation (under a 1% O_2-99% N_2 flow at room temperature) was 31 nm. This catalyst has been extensively used and a thorough characterization can be found in previous works of our research group [19, 24].

2.2 Experimental procedure

Tests were carried out in a fixed-bed quartz reactor, 15 mm i.d, 690 mm height, heated by an electric furnace. Before each test, catalyst was reduced in-situ with a H_2 flow at 550 °C for 1h. X-ray analyses of the reduced catalyst confirmed the complete reduction of the active phase (Figure not shown).

To guarantee the rate controlling regime, internal and external mass transfer limitations were analysed through the Madon-Boudart criterion [25]. To avoid difusional effects, activity tests were carried out at atmospheric pressure, with a catalyst particle size of 100-200 μm and a total feed flow rate of 12 $L_N \cdot h^{-1}$. The WHSV (Weight Hourly Space Velocity) was fixed at 1200 $L_N \cdot g_{cat}^{-1} \cdot h^{-1}$ and thus, the amount of catalyst used in each activity test was 0.01 g. The partial pressures influence was determined by keeping the partial pressure of one reactant (0.15 atm for CO_2 and 0.25 atm for CH_4) and varying the other one between 0.10 and 0.45 atm at 600 °C. N_2 was used to adjust the balance and to keep a total pressure of 1 atm. To study the temperature effect, CH_4 and CO_2 partial pressures were fixed at 0.10 atm (N_2 balanced) and temperature was varied between 600 and 700 °C. As previously stated, one of the main targets in CDB is the production of carbon nanofilaments and in [18], a thermodynamic study was carried out revealing that this temperature range was the temperature condition at which carbon formation was more favoured. Each experiment lasted one hour and allowed to determine the carbon formation effect on the catalyst activity. Table 1 shows the experimental conditions

used in each run. CH_4 and CO_2 conversions, X_i (Eq.1) and reaction rates, $(-r_i)$ (Eq.2), were calculated as follows:

$$X_i = \frac{(mole_{in,i} - mole_{out,i})}{mole_{in,i}} \ (Eq.1)$$

$$(-r_i) = \frac{X_i}{W/F_i} \ (Eq.2)$$

In Eq.1, $mole_{in,i}$ represents CH_4 or CO_2 moles introduced in the reactor and $mole_{out,i}$ represents CH_4 or CO_2 moles leaving the reactor. In Eq. 2, W represents the grams of catalyst initially loaded in the reactor and F_i, the CH_4 or CO_2 molar flow, being i: CH_4 or CO_2.

In order to determine the outlet gases composition, bag samples were taken and analysed by means of gas chromatography in a HP 5890 chromatograph equipped with two packed columns (Molecular Sieve and Porapack) and a TCD detector. Carbon samples obtained after experiments were analysed with a scanning electron microscope (SEM) (Hitachi S-3400) coupled to a Si/Li detector for energy dispersive X-ray (EDX) analysis.

3 Results and discussion

The effect of the CH_4 and CO_2 partial pressures on the Catalytic Decomposition of Biogas (CDB) initial reaction rates was studied using a Ni/Al_2O_3 catalyst. Furthermore, a deactivation study was carried out in order to determine the experimental conditions (CH_4 and CO_2 partial pressures and temperature) at which carbon formation do not deactivate the catalyst.

3.1 P_{CH4} and P_{CO2} influence: initial rates

In a first approach, reaction rates were calculated at the beginning of the reaction (initial reaction rates) to avoid carbon accumulation on the leading face of the catalyst particles. To elucidate the effect of CH_4 and CO_2 partial pressures, from now on P_{CH4} and P_{CO2} respectively, net CH_4 ($-r_{CH4}$) and CO_2 ($-r_{CO2}$) consumption rates are firstly represented as a function of P_{CO2} in Figure 1, keeping constant P_{CH4} at 0.25 atm. Initially, ($-r_{CH4}$) increased with P_{CO2} up to P_{CO2} values of 0.25 atm (CH_4:CO_2 molar ratio≥1). At higher P_{CO2}, ($-r_{CH4}$) remained almost constant (ca. 85 $mmol \cdot g_{cat}^{-1} \cdot min^{-1}$). It is likely that from 0.25 atm and onwards, the quantity of O^* produced on CO_2 decomposition reaction {4} was enough to oxidize the entire C^* formed on CH_4 decomposition reactions {1-3}, thus explaining the steady state reached by ($-r_{CH4}$) when CH_4:CO_2 molar ratio≤1. This agrees with results obtained by other authors [14, 16] which showed that when Ni active sites are the most abundant surface species, ($-r_{CH4}$) did not depend on P_{CO2}. However, at P_{CO2}<0.25 atm (CH_4:CO_2 molar ratio>1) low O^* concentration produced on reaction {4} due to the low P_{CO2}, along with high CH_4 conversions obtained (X_{CH4}>30%, Table 1) that cause a high carbon formation rate, may provoke that C^* at the surface of the catalyst cannot be considered negligible even at the beginning of the reaction. As a consequence, a reduction in the number of Ni active sites can take place, thus explaining the lower ($-r_{CH4}$) values observed.

As regard ($-r_{CO2}$), at low pressures, ($-r_{CO2}$) increased linearly until P_{CO2} reached 0.25-0.30 atm. From this pressure and onwards, ($-r_{CO2}$) remained constant. This can be tentatively explained taking into account that the amount of O^* needed to react with the entire C^* was achieved at CO_2 pressures above 0.25 atm when CH_4:CO_2 molar ratio is ≤1 and therefore reaction {4} was equilibrated provoking a constant ($-r_{CO2}$). On the other hand, at P_{CO2}<0.25 (CH_4:CO_2 molar ratio>1), even though the amount of C^* in the catalyst surface is expected to be constant since P_{CH4} is fixed at 0.25 atm, the amount of

O^* produced from CO_2 decomposition reaction {4} decreased as P_{CO2} did, explaining the decrease in ($-r_{CO2}$). Even though, RWGS {10} could influence on ($-r_{CO2}$), it is considered quasi-equilibrated in DRM [16, 17] and therefore, an important influence on ($-r_{CH4}$) and ($-r_{CO2}$) is not expected.

In Figure 2, the effect of P_{CH4} is analyzed keeping constant P_{CO2} at 0.15 atm. An increase of ($-r_{CH4}$) was observed as P_{CH4} increased. Many studies [11, 14, 16] concluded that CH_4 and/or CH_x^* decomposition are the rate determining steps (RDS) of the CH_4-CO_2 reaction and thus, an increase in P_{CH4} provokes an increase in ($-r_{CH4}$). This statement is valid as long as catalyst behaviour is not affected by C^* accumulation at the surface of the catalyst particles. In Figure 2, ($-r_{CH4}$) trend coincides with the expected one. However, and according with results presented before (Figure 1), a slight contribution of the deactivation phenomenon can take place when CH_4:CO_2 molar ratio>1 since carbon accumulation on the leading face of the catalyst could provoke a decrease of the initial ($-r_{CH4}$).

On the other hand, ($-r_{CO2}$) was constant and did not depend on P_{CH4}, excepting at P_{CH4}=0.10 atm, where a lower value was observed. At $P_{CH4}\geq$0.15 atm, ($-r_{CH4}$) increased and therefore the amount of C^* and CH^* in the surface of the catalyst particle also did. These products, in turn, react with the O^* produced on reaction {4} generating CHO^* and finally CO^*. Even if ($-r_{CO2}$) was expected to increase due to the shift of reaction {4} provoked by O^* consumption, it remained constant (ca. 60 $mmol \cdot g_{cat}^{-1} \cdot min^{-1}$). A simultaneous production of CO^* takes place (reaction {5} and {7}) and as a result reaction {4} was equilibrated. Nevertheless, when P_{CH4}=0.10 atm, the amounts of C^* and CH^* produced on CH_4 decomposition reactions {1-3} may be insufficient to react

with the O^* produced on CO_2 decomposition reaction {4} and thus the equilibrium was shifted causing a decrease of $(-r_{CO2})$.

3.2 Catalyst deactivation study

To study the catalyst deactivation phenomenon, $(-r_{CH4})$ and $(-r_{CO2})$ evolution with time were analyzed as a function of P_{CH4} and P_{CO2}, by keeping constant the other pressure. In this section, only results related with P_{CH4} are shown. Results obtained as a function of P_{CO2} (at constant P_{CH4}) were found to present the same trend as the ones obtained as a function of P_{CH4} and are therefore not included.

In Figure 3, $(-r_{CH4})$ is plotted as a function of P_{CH4} and time on stream (TOS) at 600 °C. P_{CO2} was kept constant at 0.15 atm. To complete Figure 3, $(-r_{CH4})$ and $(-r_{CO2})$ values as a function of TOS are showed in Table 2. At P_{CH4}=0.10 and 0.15 atm (dash lines), which correspond to CH_4:CO_2 molar ratio≤1, a slight deactivation was observed in the first 5 minutes of reaction. Thereafter, catalyst seemed to reach a steady state since $(-r_{CH4})$ remained almost invariable after 15, 30 and 60 minutes TOS. In these cases, it was found that $(-r_{CH4})\leq(-r_{CO2})$ and thus C^* from CH_4 decomposition reactions {1-3} can be considered to be completely removed from the leading face of the catalyst particles, avoiding encapsulation and deactivation. C^* may either diffuse to the trailing face of the catalyst particle to form filamentous carbon {11} or be oxidized by the O^* {5-6} produced on CO_2 decomposition reaction {4}.

On the other hand, from P_{CH4}=0.20 atm and onwards (CH_4:CO_2 molar ratio>1), a clear deactivation, more significant as P_{CH4} augmented, was observed in the first 5 minutes TOS. Between 15 and 30 min TOS, catalyst deactivation was still present but the drop of $(-r_{CH4})$ was less pronounced. Subsequently, $(-r_{CH4})$ remained almost constant and a

steady state was probably reached. To explain this behaviour, ($-r_{CH4}$) and ($-r_{CO2}$) have to be considered. In cases where CH_4:CO_2 molar ratio>1, initial ($-r_{CH4}$) were higher than initial ($-r_{CO2}$) (Table 2), and an accumulation of C^* on the leading face of the catalyst may take place in the first minutes reaction since the amount of O^* produced on reaction {4} was probably not enough to oxidize the entire C^*. This accumulation is expected to be greater as P_{CH4} increased, since differences between the initial ($-r_{CH4}$) and ($-r_{CO2}$) were bigger. As a consequence, a reduction of the Ni active sites can take place and hence ($-r_{CH4}$) underwent a reduction. As TOS increased (30 and 60 minutes), ($-r_{CH4}$) became more similar to ($-r_{CO2}$) and as a result, the amount of C^* produced equalled the amount of O^*.

Summarizing, ($-r_{CH4}$) decreased when deactivation occurred. This fact was more significant as the CH_4:CO_2 molar ratio increased. At P_{CH4}=0.35 atm, the initial ($-r_{CH4}$) was 83 $mmol \cdot g_{cat}^{-1} \cdot min^{-1}$ while after 60 minutes was 39 $mmol \cdot g_{cat}^{-1} \cdot min^{-1}$. A drop over a 50% took place. In contrast, if deactivation did not occur (CH_4:CO_2 molar ratio≤1), ($-r_{CH4}$) remained almost constant and even if the initial ($-r_{CH4}$) was lower compared with tests where CH_4:CO_2 molar ratio>1, after a certain TOS the trend could be reversed. For example, at P_{CH4}=0.15 atm, ($-r_{CH4}$) was approximately 60 $mmol \cdot g_{cat}^{-1} \cdot min^{-1}$ for the entire experiment. This value was higher than the one obtained at P_{CH4}=0.35 atm after 60 minutes (i.e. 39 $mmol \cdot g_{cat}^{-1} \cdot min^{-1}$). However, in biogas the CH_4:CO_2 molar ratio is usually equal or higher than one depending on the biogas source. Results here presented are very promising since it has been proved that at CH_4:CO_2 molar ratio≥1 and after a certain TOS (ca. 30 minutes), a steady state was achieved regardless the CH_4:CO_2 molar ratio.

In all the CDB experiments and regardless the CH_4:CO_2 molar ratio used, carbon formation was observed. However, a SEM micrograph of the carbon material obtained

after CDB (P_{CH4}=P_{CO2}=0.15 atm and 600 ºC) is shown in Figure 4 confirming that carbon nanofilaments formation is possible avoiding catalyst deactivation. SEM study revealed that carbon appeared as long nanofilaments few microns long with a high degree of structural order as it was proved in previous works [18, 19]. This material can be used in different areas as graphitic precursor for subsequent application as anode in the rechargeable lithium-ion batteries [26], as catalyst support in PEM fuel cells applications [27], or as additive in epoxy-based composites [28], among other applications.

3.3 Temperature effect

The effect of temperature on ($-r_{CH4}$) and ($-r_{CO2}$) was studied along with catalyst deactivation. In the previous section, it was established that CH_4-CO_2 reaction could be carried out without catalyst deactivation at 600 °C if CH_4:CO_2 molar ratio≤1. Thus, the partial pressure of both reactants, CH_4 and CO_2, was kept at 0.1 atm (N_2 balanced) in order to elucidate the temperature effect on initial reaction rates and catalyst deactivation with time. With that purpose temperature was varied from 600 to 700 °C.

In Figure 5, ($-r_{CH4}$) and ($-r_{CO2}$) at the beginning of the reaction (initial rates) are plotted as a function of temperature. The main reactions involved in the CH_4-CO_2 reaction are endothermic [29] and for that reason, when temperature increased, both ($-r_{CH4}$) and ($-r_{CO2}$) increased. Furthermore, it was observed that both reaction rates were very similar, ($-r_{CH4}$)≈($-r_{CO2}$), and according to results presented in section 3.2, deactivation is not expected. To confirm that, ($-r_{CH4}$) is represented as a function of TOS for different temperatures ranging from 600 to 700 °C in Figure 6. Firstly, a slight deactivation was observed in the first 15 minutes TOS; however, no trend was appreciated as a function of temperature. For example, the reduction of ($-r_{CH4}$) after 15 minutes at 620 °C was 8

mmol·g_{cat}^{-1}·min^{-1} (8%) while at 660 °C was 4 mmol·g_{cat}^{-1}·min^{-1} (3%) and at 700 °C was 10 mmol·g_{cat}^{-1}·min^{-1} (7%). Secondly, the drop of ($-r_{CH4}$) between 15 and 30 minutes was reduced for all the temperatures, representing a reduction of the catalyst deactivation. Finally, between 30 and 60 minutes, a steady state was almost achieved at all the temperatures studied and catalyst deactivation was negligible. Therefore, even if a slight deactivation was observed at the beginning of the reaction, after one hour TOS catalyst stability seemed to be achieved regardless of the temperature when feeding a CH_4:CO_2 molar ratio=1.

4 Conclusions

Depending on CH_4:CO_2 molar ratio, two different behaviours according to catalyst deactivation were observed. Firstly, when CH_4:CO_2 molar ratio≤1 ($P_{CH4}\leq P_{CO2}$), the amount of C* accumulated on the leading face of the catalyst was negligible and as a result, catalyst deactivation did not take place. Secondly, when CH_4:CO_2 molar ratio>1 (usual biogas conditions), a clear deactivation, more important as CH_4:CO_2 molar ratio increased, was observed at the beginning of the reaction. However, after a certain TOS, ($-r_{CH4}$) equalled ($-r_{CO2}$) and the steady state was also achieved in these conditions. Partial pressures and deactivation studies revealed that after a certain TOS and regardless the CH_4:CO_2 molar ratio, CH_4-CO_2 reaction could be carried out with a Ni/Al_2O_3 catalyst producing simultaeously syngas and filamentous carbon structures without catalyst deactivation. Besides, temperature study performed at $P_{CO2}=P_{CH4}=0.10$ atm revealed that temperature did not affect catalyst deactivation in the temperature range between 600 and 700 °C. However and due to the endothermicity of the process, an increase in the reaction rates was observed as the temperature increased.

Acknowledgments

The authors acknowledge the Spanish Economy and Competitiveness Ministry and the ERDF funds for the financial support of the Project ENE2011-28318-C03-01. S. de Llobet thanks the Diputación General de Aragón for the Ph.D. grant.

References

[1] A. Wellinger, A. Lindberg, Biogas Upgrading and utilisation, Task 24: Energy from Biological Conversion of Organic Waste (IEA Bioenergy), (2000).
[2] J.R. Rostrupnielsen, J.H.B. Hansen, CO2-Reforming of Methane over Transition Metals, J. Catal., 144 (1993) 38-49.
[3] J.H. Edwards, A.M. Maitra, The chemistry of methane reforming with carbon dioxide and its current and potential applications, Fuel Process. Technol., 42 (1995) 269-289.
[4] M.C.J. Bradford, M.A. Vannice, CO2 reforming of CH4, Catalysis Reviews, Science and Engineering, 41 (1999) 1-42.
[5] Y. Hu, E. Ruckenstein, Catalytic Conversion of Methane to Synthesis Gas by Partial Oxidation and CO2 Reforming, Advances in Catalysis, 48 (2004) 297-345.
[6] A.E. Castro Luna, M.E. Iriarte, Carbon dioxide reforming of methane over a metal modified Ni-Al2O3 catalyst, Appl. Catal., A, 343 (2008) 10-15.
[7] K. Asai, K. Takane, Y. Nagayasu, S. Iwamoto, E. Yagasaki, M. Inoue, Decomposition of methane in the presence of carbon dioxide over Ni catalysts, Chemical Engineering Science, 63 (2008) 5083-5088.
[8] D. San-José-Alonso, J. Juan-Juan, M.J. Illán-Gómez, M.C. Román-Martínez, Ni, Co and bimetallic Ni–Co catalysts for the dry reforming of methane, Appl. Catal., A, 371 (2009) 54-59.
[9] J. Xu, W. Zhou, Z. Li, J. Wang, J. Ma, Biogas reforming for hydrogen production over a Ni-Co bimetallic catalyst: Effect of operating conditions, International Journal of Hydrogen Energy, 35 (2010) 13013-13020.
[10] B. Fidalgo, J.Á. MenÉNdez, Carbon Materials as Catalysts for Decomposition and CO2 Reforming of Methane: A Review, Chinese Journal of Catalysis, 32 (2011) 207-216.
[11] Z.L. Zhang, X.E. Verykios, Carbon dioxide reforming of methane to synthesis gas over supported Ni catalysts, Catal. Today, 21 (1994) 589-595.
[12] T. Osaki, T. Horiuchi, K. Suzuki, T. Mori, Catalyst performance of MoS2 and WS2 for the CO2-reforming of CH4 Suppression of carbon deposition, Applied Catalysis A: General, 155 (1997) 229-238.
[13] S.Y. Foo, C.K. Cheng, T.-H. Nguyen, A.A. Adesina, Kinetic study of methane CO2 reforming on Co–Ni/Al2O3 and Ce–Co–Ni/Al2O3 catalysts, Catal. Today, 164 (2011) 221-226.
[14] M.C.J. Bradford, M.A. Vannice, Catalytic reforming of methane with carbon dioxide over nickel catalysts II. Reaction kinetics, Appl. Catal., A, 142 (1996) 97-122.
[15] Y. Cui, H. Zhang, H. Xu, W. Li, Kinetic study of the catalytic reforming of CH4 with CO2 to syngas over Ni/α-Al2O3 catalyst: The effect of temperature on the reforming mechanism, Applied Catalysis A: General, 318 (2007) 79-88.
[16] J. Wei, E. Iglesia, Isotopic and kinetic assessment of the mechanism of reactions of CH 4 with CO2 or H2O to form synthesis gas and carbon on nickel catalysts, J. Catal., 224 (2004) 370-383.
[17] Y.-A. Zhu, D. Chen, X.-G. Zhou, W.-K. Yuan, DFT studies of dry reforming of methane on Ni catalyst, Catal. Today, 148 (2009) 260-267.
[18] J.L. Pinilla, S. de Llobet, I. Suelves, R. Utrilla, M.J. Lázaro, R. Moliner, Catalytic decomposition of methane and methane/CO2 mixtures to produce synthesis gas and nanostructured carbonaceous material, Fuel, 90 (2011) 2245-2253.

[19] S. de Llobet, J.L. Pinilla, M.J. Lázaro, R. Moliner, I. Suelves, Catalytic decomposition of biogas to produce H2-rich fuel gas and carbon nanofibers. Parametric study and characterization, Int. J. Hydrogen Energy, 37 (2012) 7067-7076.
[20] R.T.K. Baker, M.A. Barber, P.S. Harris, F.S. Feates, R.J. Waite, Nucleation and growth of carbon deposits from the nickel catalyzed decomposition of acetylene, J. Catal., 26 (1972) 51-62.
[21] N.M. Rodriguez, A review of catalytically grown carbon nanofibers, Journal of Materials Research 8:12 (1993) 3233-3250.
[22] J.L. Pinilla, R. Moliner, I. Suelves, M.J. Lázaro, Y. Echegoyen, J.M. Palacios, Production of hydrogen and carbon nanofibers by thermal decomposition of methane using metal catalysts in a fluidized bed reactor, International Journal of Hydrogen Energy, 32 (2007) 4821-4829.
[23] I. Suelves, M.J. Lázaro, R. Moliner, Y. Echegoyen, J.M. Palacios, Characterization of NiAl and NiCuAl catalysts prepared by different methods for hydrogen production by thermo catalytic decomposition of methane, Catal. Today, 116 (2006) 271-280.
[24] J.L. Pinilla, I. Suelves, M.J. Lázaro, R. Moliner, J.M. Palacios, Influence of nickel crystal domain size on the behaviour of Ni and NiCu catalysts for the methane decomposition reaction, Appl. Catal., A, 363 (2009) 199-207.
[25] R.P. Chambers, M. Boudart, Lack of dependence of conversion on flow rate in catalytic studies, Journal of Catalysis, 6 (1966) 141-145.
[26] A.B. Garcia, I. Cameán, I. Suelves, J.L. Pinilla, M.J. Lázaro, J.M. Palacios, R. Moliner, The graphitization of carbon nanofibers produced by the catalytic decomposition of natural gas, Carbon, 47 (2009) 2563-2570.
[27] D. Sebastián, A.G. Ruíz, I. Suelves, R. Moliner, M.J. Lázaro, V. Baglio, A. Stassi, A.S. Aricò, Enhanced oxygen reduction activity and durability of Pt catalysts supported on carbon nanofibers, Applied Catalysis B: Environmental, 115–116 (2012) 269-275.
[28] R. Utrilla, J.L. Pinilla, I. Suelves, M.J. Lázaro, R. Moliner, Catalytic decomposition of methane for the simultaneous co-production of CO2-free hydrogen and carbon nanofibre based polymers, Fuel, 90 (2011) 430-432.
[29] C. Huang, A. Traissi, Thermodynamic analyses of hydrogen production from sub-quality natural gasPart I: Pyrolysis and autothermal pyrolysis, Journal of Power Sources, 163 (2007) 645-652.

Table 1. Experimental conditions of each activity test.

n^o	P_{CH4} (atm)	P_{CO2} (atm)	$W:F_{CH4}$ (g_{cat}·min·mmol^{-1})	$W:F_{CO2}$	Temp. (°C)	$CH_4:CO_2$ (-)	X_{CH4} (-)	X_{CO2} (-)
1	0.10	0.15	1.22E-02	8.15E-03	600	0.7	63	45
2	0.15		8.15E-03			1.0	50	51
3	0.20		6.11E-03			1.3	39	51
4	0.25		4.89E-03			1.7	32	50
5	0.30		4.07E-03			2.0	32	49
6	0.35		3.49E-03			2.3	27	48
7	0.40		3.06E-03			2.7	25	47
8	0.45		2.72E-03			3.0	25	50
9	0.25	0.10	4.89E-03	1.22E-02	600	2.5	30	54
10		0.15		8.15E-03		1.7	32	50
11		0.20		6.11E-03		1.3	35	47
12		0.25		4.89E-03		1.0	42	44
13		0.30		4.07E-03		0.8	43	35
14		0.35		3.49E-03		0.7	43	37
15		0.40		3.06E-03		0.6	42	32
16		0.45		2.72E-03		0.6	40	29
17	0.10	0.10	1.22E-02	1.22E-02	600	1.0	44	48
18					620		51	48
19					640		53	55
20					660		61	61
21					680		65	65
22					700		77	70

Table 2. ($-r_{CH4}$) and ($-r_{CO2}$) values as a function of TOS and P_{CH4}. P_{CO2}=0.15 atm and T=600 ºC.

P_{CH4} (atm)	**0.1**		**0.15**		**0.2**		**0.25**		**0.35**		**0.45**	
TOS (min)	**$-r_{CH4}$**	**$-r_{CO2}$**	**$-r_{CH4}$**	**$-r_{CO2}$**	**$-r_{CH4}$**	**$-r_{CO2}$**	**$-r_{CH4}$**	**$-r_{CO2}$**	**$-r_{CH4}$**	**$-r_{CO2}$**	**$-r_{CH4}$**	**$-r_{CO2}$**
					(mmol·g_{cat}^{-1}·min^{-1})							
2	52	55	62	63	64	63	66	61	78	59	92	62
3	52	55	62	63	63	62	66	61	83	61	101	62
5	49	53	58	61	61	59	59	55	58	48	58	47
15	48	53	58	60	57	56	51	49	44	38	42	40
30	48	52	58	60	51	53	44	42	39	38	38	39
60	48	51	56	59	48	50	43	41	39	38	38	37

Figure captions

Figure 1. Initial ($-r_{CH4}$) and ($-r_{CO2}$) as a function of the P_{CO2} at 600 °C (P_{CH4}=0.25 atm).

Figure 2. Initial ($-r_{CH4}$) and ($-r_{CO2}$) as a function of the P_{CH4} at 600 °C (P_{CO2}=0.15 atm).

Figure 3. ($-r_{CH4}$) as a function of the time on stream for different P_{CH4} at 600 °C (P_{CO2}=0.15 atm).

Figure 4. SEM micrograph of the carbonaceous product generated during the CH_4-CO_2 reaction (P_{CH4}=P_{CO2}=0.15 atm and 600 °C).

Figure 5. Initial ($-r_{CH4}$) and ($-r_{CO2}$) as a function of the temperature (P_{CH4}=P_{CO2}=0.10 atm).

Figure 6. ($-r_{CH4}$) as a function of the time on stream for different temperatures (P_{CH4}=P_{CO2}=0.10 atm).

Figure 1

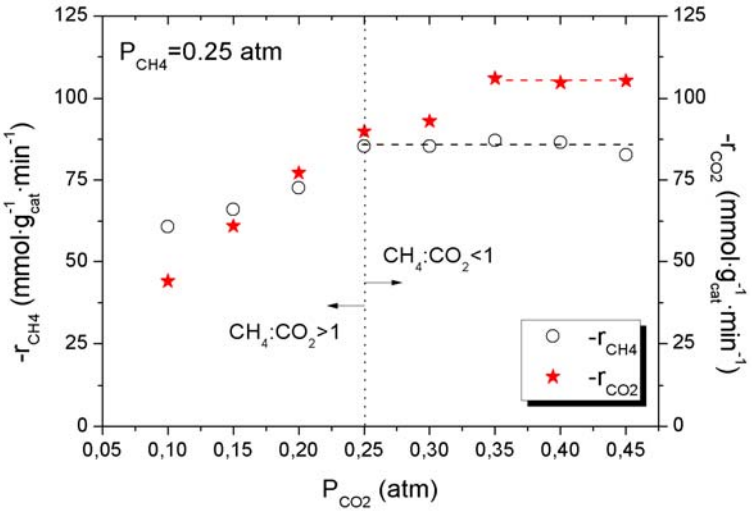
P_CH4=0.25 atm
CH4:CO2<1
CH4:CO2>1
-rCH4
-rCO2
-rCH4 (mmol·gcat-1·min-1)
-rCO2 (mmol·gcat-1·min-1)
PCO2 (atm)
0
25
50
75
100
125
0,05
0,10
0,15
0,20
0,25
0,30
0,35
0,40
0,45

Figure 2

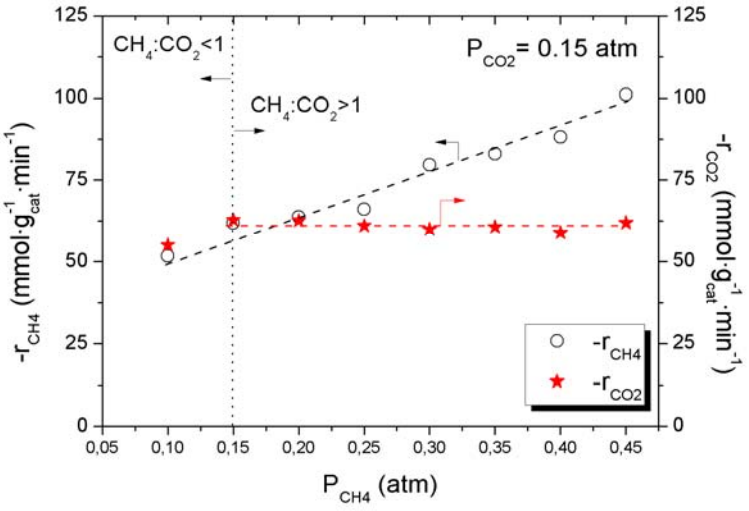
CH4:CO2<1
CH4:CO2>1
PCO2= 0.15 atm
-rCH4
-rCO2
-rCH4 (mmol·gcat-1·min-1)
-rCO2 (mmol·gcat-1·min-1)
PCH4 (atm)
125
100
75
50
25
0
0,05
0,10
0,15
0,20
0,25
0,30
0,35
0,40
0,45

Figure 3

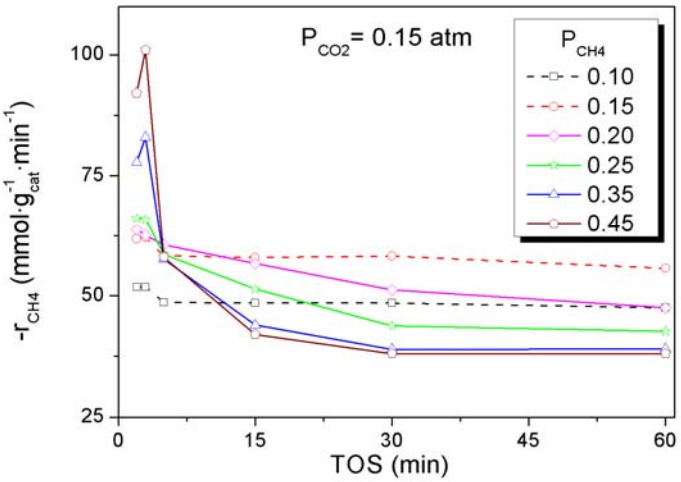
P$_{CO2}$= 0.15 atm
P$_{CH4}$
0.10
0.15
0.20
0.25
0.35
0.45
-r$_{CH4}$ (mmol·g$^{-1}_{cat}$·min^{-1})
100
75
50
25
0
15
30
45
60
TOS (min)

Figure 4

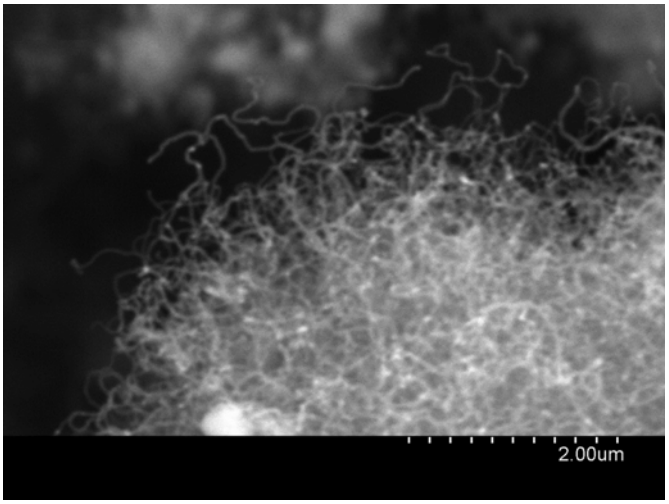

Figure 5

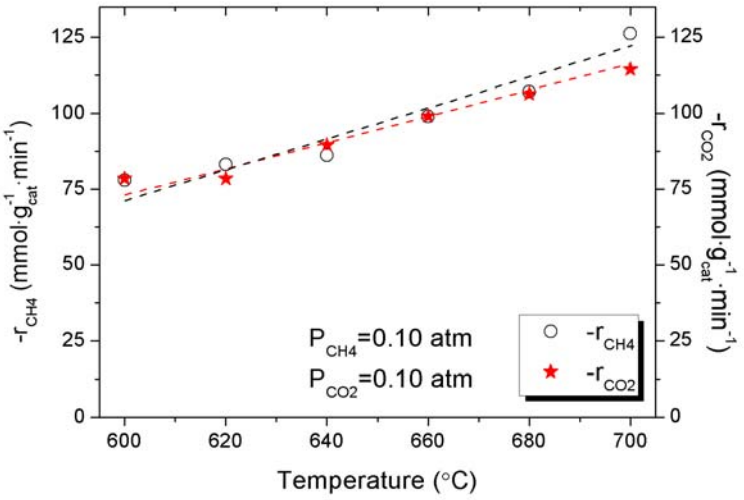
125
100
75
50
25
0
600
620
640
660
680
700
Temperature (°C)
-r_CH4 (mmol·g_cat^-1·min^-1)
-r_CO2 (mmol·g_cat^-1·min^-1)
P_CH4=0.10 atm
P_CO2=0.10 atm
-r_CH4
-r_CO2

Figure 6

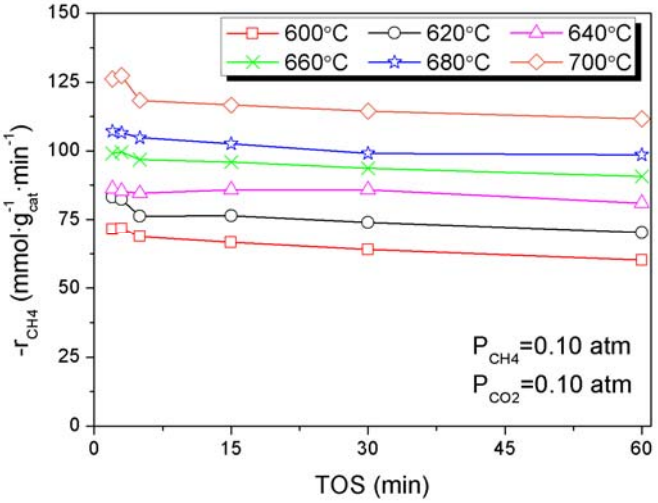
600°C
620°C
640°C
660°C
680°C
700°C
$-r_{CH4}$ (mmol·g_{cat}^{-1}·min^{-1})
TOS (min)
P_{CH4}=0.10 atm
P_{CO2}=0.10 atm
0
25
50
75
100
125
150
0
15
30
45
60